ChemMedChem

Research Article
doi.org/10.1002/cmdc.202300001

Chemistry Europe
European Chemical Societies Publishing

www.chemmedchem.org

Design of OSMI-4 Analogs Using Scaffold Hopping: Investigating the Importance of the Uridine Mimic in the Binding of OGT Inhibitors

Cyril Balsollier,[a, b] Tihomir Tomašič,[b] Daniel Yasini,[b] Simon Bijkerk,[a] Marko Anderluh,*[b] and Roland J. Pieters*[a]

β-*N*-Acetylglucosamine transferase (OGT) inhibition is considered an important topic in medicinal chemistry. The involvement of O-GlcNAcylation in several important biological pathways is pointing to OGT as a potential therapeutic target. The field of OGT inhibitors drastically changed after the discovery of the 7-quinolone-4-carboxamide scaffold and its optimization to the first nanomolar OGT inhibitor: OSMI-4. While OSMI-4 is still the most potent inhibitor reported to date, its physicochemical properties are limiting its use as a potential drug candidate as well as a biological tool. In this study, we have introduced a simple modification (elongation) of the peptide part of OSMI-4 that limits the unwanted cyclisation during OSMI-4 synthesis while retaining OGT inhibitory potency. Secondly, we have kept this modified peptide unchanged while incorporating new sulfonamide UDP mimics to try to improve binding of newly designed OGT inhibitors in the UDP-binding site. With the use of computational methods, a small library of OSMI-4 derivatives was designed, prepared and evaluated that provided information about the OGT binding pocket and its specificity toward quinolone-4-carboxamides.

Introduction

O-GlcNAcylation is an intracellular post-translational modification (PTM) that occurs on serine and threonine residues of proteins by a β-*N*-acetylglucosamine moiety. This modification is related to various biological processes ranging from enzyme activity to gene expression.[1–4] This PTM is also linked to diseases like Alzheimer's disease[5–7] and cancer.[2,8–10] Further interest in O-GlcNAcylation is derived from its crosstalk with phosphorylation by competing for the same modification site[11–13] and/or affecting each other when on nearby modification sites.[14–16] This crosstalk needs to be further deciphered to illuminate new ways of regulation.[17–19] Additionally kinase activities may be affected by the O-GlcNAcylation of kinases, providing yet another level of regulation.[20] One particularity of O-GlcNAcylation is that it is modulated by only two enzymes: O-GlcNAc transferase (OGT), which attaches the *N*-acetyl-glucosamine moiety to the target protein, and O-GlcNAcase (OGA) which removes it. While OGA is a validated therapeutic target with inhibitors in phase I clinical trials,[5] OGT inhibitors are still in very early drug-development phases, and OGT is still not a validated therapeutic target.

Many strategies were applied to design OGT inhibitors ranging from bisubstrate inhibitors,[21,22] in-cell formation of inhibitors,[23] and small molecule development through SAR and docking leading to micromolar to low micromolar affinity inhibitors.[24–26] One of these routes lead to OSMI-4, the current most potent inhibitor of OGT with a reported Kd of 8 nM.[25] While the binding affinity of this molecule is quite high, its potential off-target effects,[27] synthetic hurdles due to diketopiperazine side-product formation, and poor cellular activity ($EC_{50} = 3\ \mu M$) are less than ideal. Previously we reported that the carboxylic acid of OSMI-4, i.e. OSMI-4 carboxylate, was not essential for binding and that the ester derivative was even a slightly more potent OGT inhibitor.[28] OSMI-4 can be seen as composed of two parts : a) a peptide part, which is composed of a phenylglycine derivative linked to a glycine ester and b) the uridine mimic: quinolinon-6-sulfonamide linked through a sulfonamide (Figure 1A). In the crystal structure of the OGT-OSMI-4 carboxylate complex,[25] it makes four hydrogen bonds with the backbone structure of OGT, and two of these involve the quinolone amide of OSMI-4 and the amide carbonyl and the amide NH of Ala896 of OGT (Figure 1B). Those two hydrogen bonds are similar to those formed by uridine in the crystal structures of UDP and UDP–GlcNAc complexed with OGT. The remaining two hydrogen bonds involve one of the sulfonyl oxygens binding to both the His562 ring NH and Lys898 ammonium group. We here report on our efforts to create new analogues of OSMI-4 to block side product formation in the synthesis. Besides this, we employed a scaffold

[a] C. Balsollier, S. Bijkerk, Prof. R. J. Pieters
Department of Chemical Biology & Drug Discovery
Utrecht Institute for Pharmaceutical Sciences
Utrecht University, Universiteitsweg 99
3584 CG Utrecht (The Netherlands)
E-mail: r.j.pieters@uu.nl
[b] C. Balsollier, Dr. T. Tomašič, D. Yasini, Prof. M. Anderluh
Department of Pharmaceutical Chemistry
Faculty of Pharmacy
University of Ljubljana
1000 Ljubljana (Slovenia)
E-mail: marko.anderluh@ffa.uni-lj.si

Supporting information for this article is available on the WWW under https://doi.org/10.1002/cmdc.202300001

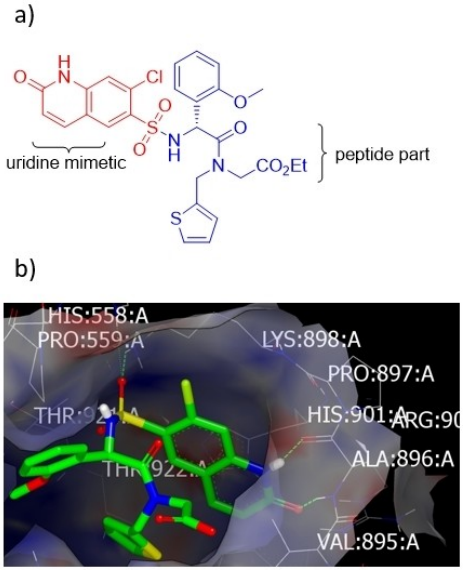

Figure 1. A) Structure of OSMI-4; B) OGT co-crystallized with OSMI-4, highlighting the hydrogen bond network upon binding PDB: 6MA1.[25]

hopping protocol with a focus on the quinolone-6-sulfonamide unit. The aim was to design a small OSMI-4-based library, with the use of an *in-silico* synthetic protocol and molecular docking. The best scoring compounds were then synthesized and assessed in an *in vitro* assay.

Results and Discussion

Design and modelling

The peptide part of OSMI-4 has a limited impact on the binding since it is not involved in any direct interaction with OGT. Clearly, the most important interactions are the ones involving the uridine mimic moiety, as shown in Figure 1A: these involve H-bonding with Ala896 and are present in various inhibitors and the natural substrate. Nevertheless, interactions to other parts can be of importance, as was shown by Goblin1, a bisubstrate micromolar inhibitor that forms an extensive hydrogen bond network with OGT as seen in the crystal structure.[22]

One possible role of the peptide part of OSMI-4 may be that it enforces a productive 3D conformation with a good match for the binding pocket. Based on this hypothesis, a peptidic inhibitor with a similar U-shape was designed and reached micromolar inhibition without a uridine mimic.[29] In the present work, the peptide part was left largely untouched, while the focus was on variations in the sulphonamide-linked quinolone moiety. These variations have led to an *in silico*-generated library. To prepare our *in silico* library of sulfonamide-based OSMI-4 analogues, we first downloaded the structures of 24.000 sulfonyl chlorides from the eMolecules database. The library of OSMI-4 analogues was then synthesized *in silico* using the RDKit Two Component Reaction node (rdkit.org) in the KNIME Analytics Platform workflow[30] to react all sulfonyl chlorides with the peptide part of OSMI-4. A conformer library of all the sulfonamides was created using OMEGA 4.2.0.1 (OpenEye Scientific Software Inc.)[31,32] and were docked into the OGT binding pocket, as derived from the OGT/OSMI-4 complex (PDB ID: 6MA1).[33] Docking was performed with the FRED module of the OpenEye software suite,[34] using two H-bond constraints, i.e. those involving Ala896, involved in UDP binding.

The docking protocol resulted in two promising groups of compounds. The first included benzene-fused heterocycles, including members such as benzo-indolinone, benzo-thiazolone, benzo-oxazolone, and benzo-imidazolinone. Interestingly, indolinones were already part of previously reported OGT inhibitors.[33] The second group was based on the 1*H*-pyrrolo[2,3-*b*]pyridine heterocycle, which was not part of previous OGT inhibitors.

Synthesis

In a former study[28] our group identified the formation of a diketopiperazine side product during the synthesis of OSMI-4. This side product is formed by intramolecular cyclization involving the nitrogen of the sulfonamide and the ester carbonyl. The nitrogen is deprotonated under basic conditions, allowing the cyclization. Since the resulting diketopiperazine showed greatly reduced inhibition of OGT, this reaction pathway should be avoided when synthesizing OSMI-4 derivatives. Our strategy to eliminate the biproduct was to elongate the glycine chain by one methylene starting the synthesis from β-Alanine. This would lead to a 7-member ring cyclization, a less favorable cyclization than the original one leading to a 6-member ring.

The new synthesis (Scheme 1) started with the esterification of β-alanine **1**, instead of glycine, introducing the extra carbon at an early stage of the synthesis. Subsequent steps were according to our previously published protocol[33] with the reductive amination by thiophene-2-carboxaldehyde, amidation of the resulting **3** with (R)-2-((*tert*-butoxycarbonyl)amino)-2-(2-methoxyphenyl) acetic acid and formation of the sulfonamide by reacting the newly formed peptide part with sulfonyl chloride **6** to give the final ester **7.** This was hydrolyzed with aqueous lithium hydroxide to give the carboxylic acid **8**, gratifyingly without formation of any cyclized side product. For the synthesis of the library, compound **5** was coupled with the selected sulfonyl chlorides using the same method as for **6** and OSMI-4. The resultant series (**9**–**15**) is shown in Figure 2.

Evaluation

For the evaluation we used the assay published by the Vocadlo group[35] under the same conditions as reported before.[33] The IC_{50} of **7** was 69 nM, which is similar to our previously reported IC_{50} of OSMI-4 of 60 nM confirming that the elongation of the alkyl chain did not affect the potency of the inhibitor. This was expected since the carboxylate or ester moiety in OSMI-4 point towards solvent (evident from PDB ID: 6MA1) and forms no

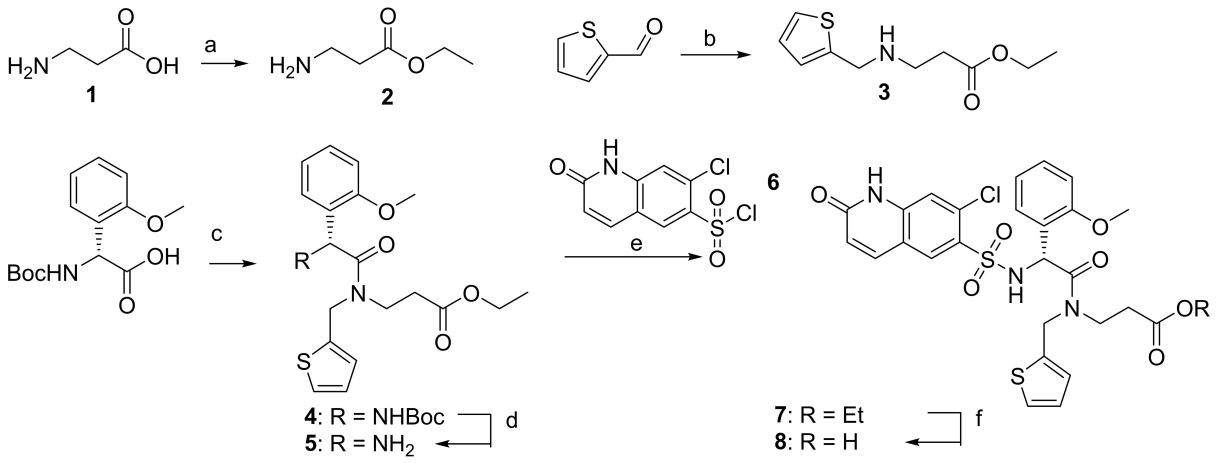

Scheme 1. Synthesis of the elongated OSMI-4 derivative **8**. a) $SOCl_2$, EtOH, 14 h, quantitative b_1) EtN_3, EtOH, 90 min b_2) $NaBH_4$, 14 h 53% over 2 steps c) HATU, DIPEA, DMF 85% d) HCl, dioxane, 1 h, quantitative e) DIPEA, DMF, 14 h, 54% f) LiOH, MeOH/water, 2 h, quantitative.

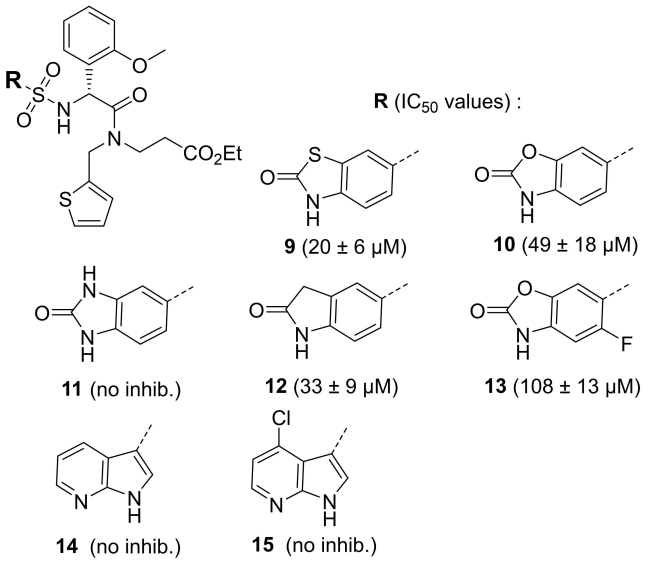

Figure 2. Molecules synthesized from the *In Silico* library and inhibitory potencies (IC_{50}) depicted between brackets. No inhibition indicates no variation of the signal at 300 μM of inhibitor.

evident interactions with OGT. Of the synthesized series, compounds **14** and **15** (Figure 2), containing the pyrrolopyridine moiety, showed no measurable inhibitory activity against OGT at 300 μM, which suggests that pyrrolopyridine fails to form the specific H-bonding with Ala896 and Val895 unlike the modelling indicated. The imidazolinone **11** also showed no inhibition of OGT. In contrast, the closely related oxazolone **10** and **13** showed binding with IC_{50}'s of 49 and 108 μM respectively. The difference between these two compounds indicates that the added fluorine substituent of **13** reduced the inhibition. The most potent molecules from the screening turned out to be indolinone **12** and thiazolinone **9** with IC_{50}'s of 33 and 20 μM.. Interestingly, all identified OGT inhibitors were ranked among top 16 compounds in the virtual screening (scoring function scores between −11.9041 and −10.8803), while inactive compounds **11**, **14** and **15** had lower scores (below −10.8) (Table S1).

Modeling refinement

The sizeable reduction of inhibitory potency of the synthesized library versus OSMI-4 was striking. We looked to modeling for answers by using two different computational tools from the OMEGA package. The first tool is POSIT which is a pose-prediction tool based on the assumption that similar ligands bind similarly to the target. Since our molecules are made to be similar to OSMI-4 POSIT would provide more information than FRED concerning the similarities between the two ligands. The second tool is FREEFORM which is used to calculate energy related to the ligand and provide in our case useful information like the desolvation penalty.

POSIT was used to dock the library to OGT as derived from its complex with OSMI-4-carboxylate in the PDB file 6MA1. Along with the library of compounds OSMI-4 was included to verify the model from POSIT. The POSIT pose found for OSMI-4-carboxylate mimicked the X-ray structure with an RMSD of 0.28 Å and upon scoring with ScorePose obtained a Chem-Gauss4 score of −12.55. With these high indications that OSMI-4 was docked in accordance with the crystal structure by POSIT (Figure S9), we went forward with the study of the other molecules.

For compounds **14** and **15** the original docking (using Fred) predicted the possibility for simultaneous binding of peptide and UDP-mimic part. Using POSIT it became clear that this is not possible, and binding of the peptide part would disrupt binding of the UDP-mimic part (see Figure S15 and S16), a result in line with the experimental data.

For the **9–13** series this was not an issue. POSIT found related binding poses to OSMI-4. To find the reduced potency of these compounds compared to OSMI-4, analyzing the POSIT model, revealed a large difference in the hydrogen bond length

and geometry between the carbonyl of the UDP mimic and Ala896. While for OSMI-4 the POSIT generated distance was 2.82 Å, between the two heavy atoms defining the hydrogen bond. This is significantly shorter than those found for **9, 10**, and **12** with distances of 3.28 Å, 3.52 Å, and 4.18 Å respectively (Figure 3). All this points to a preferred 6-membered ring geometry of this part of the molecule. Notably the length of the other hydrogen bond involving Ala-896 did not vary to the same extent.

After this, still the mystery of the inactivity of **11** remained. Measuring its UV activity in solution ruled out insolubility of the compound. According to the modelling module FREEFORM, **11** has to incur a 4.5 kcal/mol higher desolvation penalty upon binding compared to **9**, which could explain its low potency. While for **9** the cost of the desolvation is more evenly spread throughout the molecule, for **11** the lion's share resides at the benzimidazole moiety and as mentioned it is also significantly larger (Figure S18).

Conclusion

This study aimed to investigate the particularity of OSMI-4 derivatives by keeping the peptide part and exchanging the 6S-quinoline with other UDP mimics found through *in silico* synthesis. After the computational process, 2 scaffolds were selected as hits and their analogs synthesized. Unfortunately, none of those 2 analogs matched the potency of OSMI-4. After further investigation using computational tools, we saw that the pyrrolo-pyridine family does not conserve the hydrogen bond network of the uridine mimic and the 3D conformation of the peptide part, explaining why these seemingly promising compounds ended up inactive. Concerning the second family containing benzo-imidazolinone, benzo-thiazolinone, and benzo-indolinone, we were able to see in our model that a 5-member ring instead of a 6-member ring would make the hydrogen bond between the inhibitor and Ala896 less strong thus leading to activity in the micromolar range. The development of future uridine mimic inhibitors should take that hydrogen bond distance and orientation into account, while OSMI-4 clearly additionally benefits from its chlorine substituent improving the fit. As such the value of the modelling tools for the analyses of binding poses is clear and will help in the future. While OSMI-4 is a potent compound, especially its cellular activity limits its application as a biological tool to validate the therapeutic potential of OGT inhibition. In the previous study,[28] we showed that the terminal carboxylic acid is not necessary to inhibit OGT in cells, by extending the alkyl chain leading to this carboxylic acid we have shown that the chain is pointing out to the solvent and that extending it does not affect the potency. This leaves the door open to improve the overall cell permeability.

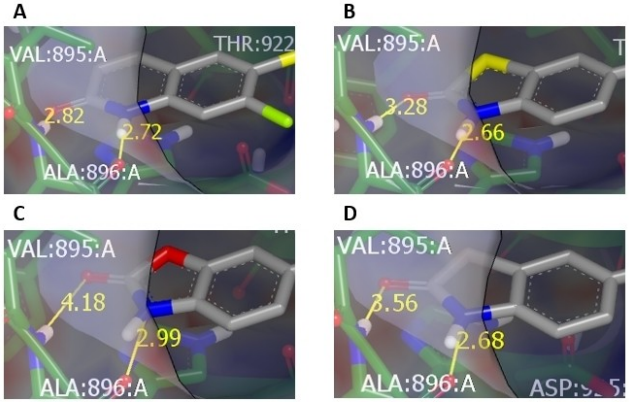

Figure 3. Comparison of the distance between the carbonyl of the inhibitor in the POSIT model and Ala896. A) OSMI-4, B) **9**, C) **10**, D) **12.**

Experimental Section

Fluorescence intensity assay. OGT reactions were carried out in a 25-μL final volume, containing 2.8 μM glycosyl donor BFL–UDP–GlcNAc, 1.6 μM purified full-length OGT, 9.2 μM glycosyl acceptor HCF-1 Serine in OGT reaction buffer (1×PBS pH 7.4, 1 mM DTT, 12.5 mM $MgCl_2$). Reactions were incubated at room temperature for 1 h, in the presence of different concentrations of inhibitor (the inhibitors were preincubated with OGT for at least 5 min). The reactions were then stopped by the addition of UDP at a final concentration of 10 mM, followed by Nanolink magnetic streptavidin beads (3 μL). After incubation at room temperature for 30 min, the beads were immobilized on a magnetic surface and washed thoroughly with PBS-tween 0.01%. Finally, the beads were resuspended in PBS-tween 0.01% and transferred to a microplate for endpoint fluorescence measurement. Fluorescence was read at Ex/Em 485/530 with a POLARstar® Omega microplate reader (BMG LABTECH). The data were plotted with GraphPad prism software, version 8, [Inhibitor] vs. response-variable slope. All IC_{50} were measured in two independent experiments. Each experiments is issued with 3 technical replicates.

UV solubility test. Different solutions of inhibitors in a concentration range between 300 μM to 3 nM were made in the same reaction buffer as the Fluorescence intensity assay (1×PBS pH 7.4, 1 mM DTT, 12.5 mM $MgCl_2$). 25 μL of these solutions is transferred in a 96 well-plates in triplicates. The UV signal is then measured by a POLARstar® Omega microplate reader (BMG LABTECH).

Docking. For docking with FRED software (Release 3.2.0.2, OpenEye Scientific Software, Inc., Santa Fe, NM, USA; **www.eyesopen.com**), the UDP–GlcNAc binding site in OGT (PDB entry: 6MA1)was prepared using MAKE RECEPTOR (Release 3.2.0.2, OpenEye Scientific Software, Inc., Santa Fe, NM, USA; **www.eyesopen.com**). The grid box around the OSMI-4a bound in the OGT crystal structure was generated automatically. This resulted in a box with the following dimensions: 16.00 Å ×21.00 Å ×18.00 Å and a volume of 6048 $Å^3$. For "Cavity detection", a slow and effective "Molecular" method was used for the detection of binding sites. The inner and outer contours of the grid box were also calculated automatically using the "Balanced" settings for the "Site Shape Potential" calculation. The inner contours were disabled. Ala896 was defined as the hydrogen bond donor and acceptor constraint for the docking calculations. The co-crystallized ligand OSMI-4a was docked to the prepared receptor using FRED (Release 3.2.0.2. OpenEye Scientific Software, Inc., Santa Fe, NM, USA) with an RMSD of 1.45 Å, thus validating the docking protocol. The small molecule library, prepared by OMEGA, was then docked at the prepared UDP–GlcNAc-binding site of OGT (PDB entry: 6MA1) using FRED. The docking resolution was set to high, other settings were set as

default. A hit list of the top 1000 ranked molecules was retrieved, and the best ranked FRED-calculated pose for each compound was inspected visually and used for analysis and representation. POSIT calculations were performed using the same receptor with default settings and -outputall enabled. The compound library was prepared using OMEGA with "maxconfs" set to 4000. The poses were scored with ScorePose on default settings. FREEFORM was run on all compounds with -calc set to "solv" and -ionic to "input".

Synthesis

^{1}H and ^{13}C NMR were performed on an Agilent 400-MR or a Bruker 600 Ultra Shield spectrometer. Chemical shifts (δ) are expressed in parts per million (ppm) relative to internal tetramethylsilane (TMS); coupling constants (J) are reported in Hz. Mass spectra were run on a Bruker micrOTOF-QII spectrometer. Preparative HPLC of final compounds were performed on a Shimadzu LC-8A preparative liquid chromatograph system with a Gilson 215 fraction collector on a C18 column on a water/acetonitrile system. HPLC analytics were run on a Shimadzu LC-10AT vp system on a C18 column paired with a preparative column. Sulfonyl chloride fragments were purchased from Enamine. Unless stated otherwise, starting materials used were high-grade commercial products.

Ethyl-3-aminopropanoate (2): β-Alanine **1** (3 g, 33 mmol) was dissolved in a mix of EtOH (100 mL) and thionyl chloride (20 mL). The reaction was then stirred at 25 °C for 2 h. The product formed is then precipitated by adding cold diethyl ether. The precipitate is then filtrated under vacuum and washed 4 times with cold Et_2O (10 mL). The resulting white solid is dried under vacuum leading to 3.9 g of a white solid (quantitative).^{1}H NMR (600 MHz, $CDCl_3$, δ) 4.28 (q, *J* = 6.7 Hz, 2H), 3.21 (t, *J* = 7.1 Hz, 2H), 2.50 (t, *J* = 7.1 Hz, 2H), 1.24 (t, *J* = 7.1 Hz, 3H).

Ethyl-3((tiophen-2-ylmethyl)amino)propanoate (3): Ethyl-3-aminopropanoate (**2**, 2.0 g, 17 mmol) was dissolved in EtOH (100 mL) and Et_3N (2.4 mL, 17 mmol) was added via syringe, followed by thiophene 2-carboxaldehyde (0.85 mL, 9.4 mmol). The reaction was stirred for 2 h at 40 °C, then allowed to cool down to 0 °C using an ice bath. Sodium borohydride (1.3 g, 34 mmol) was slowly added to the mixture, then the ice bath was removed and the reaction was stirred at r.t. overnight. A black precipitate was filtered off and the filtrate was concentrated under reduced pressure. The residue was partitioned between EtOAc (50 mL) and H_2O (50 mL). The organic layer was washed with H_2O (2×40 mL) and brine (40 mL), then dried with Na_2SO_4. EtOAc was removed *in vacuo* and the residue was purified using flash silica chromatography, eluting with 5–50% EtOAc/Hexanes to yield 1.92 g (53%) of **3** as a yellow oil. ^{1}H NMR (600 MHz, $CDCl_3$ δ) 7.51(dd, J = 4.8, 1.5 Hz, 1H), 7.09 (d, 1H), 6.82 (t, 1H) 4.12 (q, J = 7.1 Hz, 2H), 3.44 (s, 2H), 3.2 (t, J = 0.7 Hz, 2H) 2.5 (t, J = 0.7 Hz, 2H) 1.28 (t, J = 7.1 Hz, 3H).

Ethyl (R)-3-(2-((*tert*-butoxycarbonyl)amino)-2-(2-methoxyphenyl)-*N*-(thiophen-2-ylmethyl)acetamido)propanoate (4): (R)-2-((*tert*-butoxycarbonyl)amino)-2-(2-methoxyphenyl)acetic acid (450 mg, 1,71 mmol) and **3** (364 mg, 1,71 mmol) were cooled to 0 °C under argon atmosphere for 10 minutes. Dimethylformamide (DMF, 12 mL) was added via syringe, followed by 1-[Bis(dimethylamino)methylene]-1H-1,2,3-triazolo[4,5-b]pyridinium 3- oxide hexafluorophosphate (HATU) (715 mg, 1,88 mmol) by briefly removing the septum cap. Diisopropylethylamine (328 μL, 1,88 mmol) was added via syringe, and the reaction was stirred at r.t. overnight. The reaction mixture was partitioned between EtOAc (10 mL) and H_2O (10 mL). The H_2O layer was extracted with fresh EtOAc (2×10 mL). The organic layers were combined, washed with brine (10 mL), dried over Na_2SO_4, and concentrated under reduced pressure. The residue was purified by flash chromatography, eluting with 30–50% EtOAc/Hexanes to yield 690 mg (85%) of **4** as a light yellow oil (mixture of rotamers). ^{1}H NMR (600 MHz, DMSO-d_6 δ) 7.47–7.38 (m, 1H), 7.36–7.19 (m, 2H), 7.06–6.77 (m, 4H), 5.79 (dd, J = 8.9 Hz, 1H), 4.73–4.53 (m, 3H), 4.17–3.98 (m, 4H), 3.4 (t, J = 6.2 Hz, 2H) 2.6 (t, J = 6.2 Hz, 2H), 1.36 (s, 9H), 1.16–1.09 (m, 3H).

Ethyl (R)-3-(2-amino-2-(2-methoxyphenyl)-*N*-(thiophen-2-ylmethyl) acetamido) propanoate Ethyl (R)-3-(2-amino-2-(2-methoxyphenyl)-*N*-(thiophen-2-ylmethyl) acetamido) propanoate (5): A solution of HCl in dioxane (4 M, 5 mL) was added to **4** (200 mg, 0.53 mmol) at 0 °C under argon atmosphere. The reaction was stirred at r.t. for 1 h, then it was concentrated under reduced pressure to yield compound **5** as a clear oil in quantitative yield. ^{1}H NMR (400 MHz, DMSO-d_6) δ 7.50–7.39 (m, 1H), 7.37–7.23 (m, 2H), 7.06–6.85 (m, 4H), 5.85 (dd, J = 8.7 Hz, 1H), 4.73–4.53 (m, 2H), 4.17–3.98 (m, 3H), 3.6 (t, J = 6.2 Hz, 2H) 3.76 (d, J = 6.2 Hz, 3H), 1.16–1.09 (m, 3H).

Standard protocol for formation of the sulfonamides: Sulfonyl chloride (1 equiv) was dissolved in dry dimethylformamide (2.5 mL) under an argon atmosphere. A solution of compound **5** (1 equiv) in dry DCM was added dropwise to the DMF followed by DIPEA (150 μL). The reaction was stirred at r.t. overnight and then concentrated under vacuum. The residue was partitioned between EtOAc and water. The water phase was extracted with more EtOAc, then the organic layers were combined, washed with brine, dried over Na_2SO_4 and concentrated under reduced pressure. The resulting oil was purified by flash chromatography with silica as a stationary phase, eluting with 25–60% EtOAc/toluene.

Ethyl-(R)-3-(2-((7-chloro-2-oxo-1,2-dihydroquinoline)-6-sulfonamido)-2-(2-methoxyphenyl)-N-(thiophen-2-ylmethyl)acetamido)propanoate (7): ^{1}H NMR (400 MHz, DMSO) δ 12.06–11.97 (m, 1H), 8.21–8.07 (m, 2H), 8.00–7.90 (m, 1H), 7.44–7.30 (m, 1H), 7.27–7.08 (m, 3H), 6.96–6.78 (m, 3H), 6.76–6.52 (m, 2H), 5.75–5.58 (m, 1H) 4.62–4.44 (m, 2H), 4.05–3.90 (m, 2H), 3.51–3.45 (m, 3H), 3.34–3.15 (m, 2H), 2.44–1.79 (m, 2H), 1.20–1.06 (m, 3H). ^{13}C NMR (100 MHz, DMSO) δ 170.71, 168.57, 161.86, 155.12, 141.68, 139.78, 139.17, 132.11, 130.88, 130.60, 129.90, 128.61, 126.93, 126.44, 126.19, 123.54, 123.38, 123.20, 120.62, 116.96, 110.70, 60.13, 55.43, 50.43, 44.22, 41.60, 31.69, 14.02.

Ethyl-(R)-3-(2-(2-methoxyphenyl)-2-((2-oxo-2,3-dihydrobenzo[d]thiazole)-6-sulfonamido)-N-(thiophen-2-ylmethyl)acetamido)propanoate (9): ^{1}H NMR (400 MHz, $CDCl_3$) δ 10.27 (d, *J* = 167.4 Hz, 1H), 7.78 (s, 1H), 7.69–7.48 (m, 2H), 7.19 (ddd, *J* = 17.0, 13.2, 7.8 Hz, 3H), s6.96 (d, *J* = 8.4 Hz, 1H), 6.93–6.76 (m, 4H), 6.62 (d, *J* = 7.7 Hz, 1H), 6.42 (d, *J* = 7.9 Hz, 1H), 6.01 (dd, *J* = 18.4, 7.9 Hz, 1H), 4.74 (d, *J* = 14.9 Hz, 1H), 4.68–4.57 (m, 1H), 4.48 (d, *J* = 16.4 Hz, 1H), 4.08 (dt, *J* = 23.6, 7.1 Hz, 2H), 3.79 (d, *J* = 7.8 Hz, 3H), 2.44 (t, *J* = 5.8 Hz, 2H), 1.62 (s, 1H), 1.21 (dt, *J* = 22.8, 7.1 Hz, 3H). ^{13}C NMR (101 MHz, $CDCl_3$) δ 171.40, 169.82, 155.69, 138.57, 135.21, 130.34, 128.41, 128.04, 126.90, 126.49, 126.34, 126.00, 125.72, 125.58, 123.82, 123.46, 121.93, 121.36, 121.20, 110.93, 60.72, 60.59, 55.60, 55.48, 53.25, 51.32, 46.20, 44.80, 42.63, 42.16, 32.48, 31.90, 14.02, 13.96. HRMS (ESI/Q-TOF) m/z: $[M+H]^+$ Calcd for $C_{26}H_{27}N_3O_7S_3$ 589.1011; Found 589.1012. HPLC analytics C18 t_R 36 mn 100% (254 nm) 98.2% (214 nm).

Ethyl-(R)-3-(2-(2-methoxyphenyl)-2-((2-oxo-2,3-dihydrobenzo[d]oxazole)-6-sulfonamido)-N-(thiophen-2-ylmethyl)acetamido)propanoate (10): ^{1}H NMR (400 MHz, $CDCl_3$) δ 7.50 (d, *J* = 8.3 Hz, 1H), 7.25–7.17 (m, 2H), 7.13 (dd, *J* = 12.4, 7.6 Hz, 1H), 6.93 (d, *J* = 8.2 Hz, 1H), 6.91–6.78 (m, 3H), 6.78–6.71 (m, 2H), 6.41 (d, *J* = 7.5 Hz, 1H), 6.30 (d, *J* = 7.8 Hz, 1H), 5.91–5.78 (m, 1H), 4.63 (s, 1H), 4.58 (d, *J* = 16.7 Hz, 1H), 4.46 (d, *J* = 16.4 Hz, 1H), 4.08 (dt, *J* = 24.4, 8.3 Hz, 2H), 3.78 (s, 3H), 3.70–3.54 (m, 2H), 3.54–3.30 (m, 2H), 2.42 (t, *J* = 6.7 Hz, 1H), 1.30–1.21 (m, 3H). ^{13}C NMR (101 MHz, $CDCl_3$) δ

170.62, 169.78, 155.83, 142.81, 138.42, 130.26, 128.55, 128.19, 126.96, 126.47, 126.00, 125.81, 124.21, 123.97, 121.51, 109.55, 109.23, 60.89, 60.74, 55.70, 55.56, 51.23, 46.31, 44.67, 32.60, 14.20. HRMS (ESI/Q-TOF) m/z: $[M+H]^+$ Calcd for $C_{26}H_{27}N_3O_8S_2$ 573.1240; Found 573.1240. HPLC analytics C18 t_R 34.8 mn 100% (254 nm) 100% (214 nm).

Ethyl-(R)-3-(2-(2-methoxyphenyl)-2-((2-oxo-2,3-dihydro-1H-benzo[d]imidazole)-5-sulfonamido)-N-(thiophen-2-ylmethyl)acetamido)propanoate (11): ^{1}H NMR (400 MHz, DMSO) δ 10.94 (d, *J* = 25.8 Hz, 2H), 8.25 (s, 1H), 7.34 (d, *J* = 4.7 Hz, 1H), 7.30–7.11 (m, 4H), 6.94 (d, *J* = 14.8 Hz, 1H), 6.90–6.74 (m, 4H), 5.66 (d, *J* = 35.0 Hz, 1H), 4.65–4.40 (m, 2H), 4.12–3.86 (m, 2H), 3.75 (d, *J* = 12.3 Hz, 1H), 3.60 (s, 3H), 2.27–2.01 (m, 1H), 1.14 (dt, *J* = 23.9, 7.0 Hz, 3H). ^{13}C NMR (101 MHz, $CDCl_3$) δ 172.57, 169.74, 153.73, 142.81, 132.42, 128.76, 124.53, 122.39, 127.97, 123.47, 122.12, 124.80, 124.80 124.97, 121.00, 110.55, 109.73, 64.65, 61.57, 55.78, 54.96, 52.23, 46.20, 43.97, 31.64, 12.29. HRMS (ESI/Q-TOF) m/z: $[M+H]^+$ Calcd for $C_{25}H_{26}N_4O_7S_2$ 558.1240; Found 558.1242. HPLC analytics C18 t_R 30.7 mn 100% (254 nm) 96.5% (214 nm).

Ethyl-(R)-3-(2-(2-methoxyphenyl)-2-((2-oxoindoline)-5-sulfonamido)-N-(thiophen-2-ylmethyl)acetamido)propanoate (12): ^{1}H NMR (400 MHz, $CDCl_3$) δ 8.99 (d, *J* = 32.5 Hz, 1H), 7.65 (d, *J* = 8.3 Hz, 1H), 7.55 (d, *J* = 8.2 Hz, 1H), 7.41 (s, 1H), 7.17 (dt, *J* = 17.6, 10.3 Hz, 3H), 6.91–6.79 (m, 3H), 6.79–6.68 (m, 3H), 6.56 (d, *J* = 7.7 Hz, 1H), 6.40 (d, *J* = 7.9 Hz, 1H), 5.77 (dd, *J* = 19.7, 7.8 Hz, 1H), 4.57 (d, *J* = 23.7 Hz, 2H), 4.46 (s, 1H), 4.22–3.91 (m, 3H), 2.39 (t, *J* = 6.8 Hz, 2H), 1.28–1.22 (m, 4H), 1.21–1.15 (m, 2H). ^{13}C NMR (101 MHz, $CDCl_3$) δ 177.33, 177.25, 171.75, 170.78, 169.78, 169.55, 155.93, 155.88, 146.21, 138.96, 138.64, 134.40, 134.18, 130.21, 130.16, 128.71, 128.37, 127.12, 126.99, 126.62, 126.58, 126.04, 125.82, 125.46, 124.66, 124.38, 123.89, 121.55, 121.35, 111.33, 110.96, 109.21, 60.96, 60.83, 60.55, 55.81, 55.64, 51.28, 51.19, 46.31, 44.70, 42.79, 42.03, 35.89, 32.78, 32.15, 29.82, 21.19, 14.32, 14.25. HRMS (ESI/Q-TOF) m/z: $[M+H]^+$ Calcd for $C_{27}H_{29}N_3O_7S_2$ 571.1447; Found 571.1447. HPLC analytics C18 t_R 35.4 mn 100% (254 nm) 100% (214 nm).

Ethyl-(R)-3-(2-((5-fluoro-2-oxo-2,3-dihydrobenzo[d]oxazole)-6-sulfonamido)-2-(2-methoxyphenyl)-N-(thiophen-2-ylmethyl)acetamido)propanoate (13): ^{1}H NMR (600 MHz, DMSO) δ 7.83 (d, *J* = 1.9 Hz, 1H), 7.68 (d, *J* = 1.9 Hz, 0H), 7.55 (dd, *J* = 8.4, 1.9 Hz, 1H), 7.52–7.45 (m, 1H), 7.37–7.33 (m, 1H), 7.25–7.13 (m, 2H), 7.06 (dd, *J* = 8.4, 5.3 Hz, 1H), 6.99 (dd, *J* = 5.1, 3.4 Hz, 0H), 6.90–6.86 (m, 2H), 6.86–6.76 (m, 2H), 5.70 (dd, *J* = 48.8, 5.8 Hz, 1H), 4.63–4.44 (m, 2H), 4.10–3.90 (m, 2H), 3.61 (d, *J* = 15.6 Hz, 3H), 1.15 (dt, *J* = 35.5, 7.1 Hz, 3H). ^{13}C NMR (151 MHz, DMSO) δ 169.30, 140.29, 139.60, 135.62, 127.22, 126.98, 126.77, 125.81, 124.23, 121.97, 120.85, 111.41, 111.04, 60.62, 60.45, 56.01, 55.83, 50.57, 50.31, 14.53. HRMS (ESI/Q-TOF) m/z: $[M+H]^+$ Calcd for $C_{26}H_{26}FN_3O_8S_2$ 591.1145; Found 591.1146. HPLC analytics C18 t_R 34.8 mn 100% (254 nm) 100% (214 nm).

Ethyl-(R)-3-(2-(2-methoxyphenyl)-2-(1H-pyrrolo[2,3-b]pyridine-3-sulfonamido)-N-(thiophen-2-ylmethyl)acetamido)propanoate (14): ^{1}H NMR (400 MHz, $CDCl_3$) δ 11.88 (d, *J* = 17.1 Hz, 1H), 8.36 (dt, *J* = 4.9, 1.5 Hz, 1H), 8.25–8.10 (m, 1H), 7.60 (s, 1H), 7.24–6.99 (m, 5H), 6.92–6.53 (m, 5H), 5.78 (d, *J* = 7.7 Hz, 1H), 4.61–4.38 (m, 2H), 4.02 (dqd, *J* = 21.4, 7.1, 1.5 Hz, 2H), 3.58 (d, *J* = 2.1 Hz, 3H), 3.44–3.31 (m, 1H), 2.44–2.24 (m, 2H), 1.26 (s, 2H), 1.17 (dt, *J* = 17.6, 7.2 Hz, 4H). ^{13}C NMR (101 MHz, $CDCl_3$) δ 171.65, 170.68, 169.79, 169.66, 155.59, 155.51, 147.94, 143.85, 143.82, 138.91, 138.64, 130.23, 130.20, 129.91, 129.84, 129.26, 128.46, 128.17, 126.90, 126.68, 126.38, 126.29, 125.84, 125.62, 124.49, 124.21, 121.19, 120.96, 117.77, 116.94, 116.88, 114.29, 113.96, 110.97, 110.57, 60.77, 60.63, 55.42, 55.27, 51.14, 51.03, 46.24, 44.55, 42.73, 41.92, 32.65, 31.99, 29.70, 14.16, 14.10. HRMS (ESI/Q-TOF) m/z: $[M+H]^+$ Calcd for $C_{26}H_{28}N4O_6S_2$ 556.1450; Found 556.1452. HPLC analytics C18 t_R 32.1 mn 100% (254 nm) 98.7% (214 nm).

Ethyl-(R)-3-(2-((4-chloro-1H-pyrrolo[2,3-b]pyridine)-3-sulfonamido)-2-(2-methoxyphenyl)-N-(thiophen-2-ylmethyl)acetamido)propanoate (15): ^{1}H NMR (400 MHz, DMSO) δ 12.71 (dd, *J* = 9.8, 3.0 Hz, 1H), 8.21 (dd, *J* = 5.2, 2.3 Hz, 1H), 7.95 (d, *J* = 3.0 Hz, 1H), 7.34–7.27 (m, 1H), 7.25 (d, *J* = 5.1 Hz, 1H), 7.21 (dd, *J* = 7.9, 1.7 Hz, 1H), 7.04 (ddd, *J* = 8.5, 7.5, 1.7 Hz, 1H), 6.87–6.77 (m, 2H), 6.71–6.64 (m, 2H), 5.65 (dd, *J* = 12.3, 8.8 Hz, 1H), 4.60–4.44 (m, 2H), 4.07–3.90 (m, 2H), 3.51 (s, 3H), 1.84 (ddd, *J* = 16.4, 9.6, 5.1 Hz, 1H), 1.12 (dt, *J* = 14.4, 7.1 Hz, 3H). ^{13}C NMR (101 MHz, DMSO) δ 171.42, 170.84, 169.40, 155.44, 150.00, 145.14, 140.22, 134.92, 133.74, 129.89, 128.78, 127.36, 127.19, 126.82, 126.74, 126.60, 124.44, 120.83, 120.70, 118.71, 114.01, 113.78, 110.90, 60.55, 60.45, 55.72, 55.61, 50.69, 43.92, 41.85, 32.57, 31.75, 14.51, 14.44. HRMS (ESI/Q-TOF) m/z: $[M+H]^+$ Calcd for $C_{26}H_{27}ClN_4O_6S_2$ 590.1061; Found 590.1061. HPLC analytics C18 t_R 34.4 mn 97.9% (254 nm) 94.1% (214 nm).

Synthesis of (*R*)-3-(2-((7-chloro-2-hydroxyquinoline)-6-sulfonamido)-2-(2-methoxyphenyl)-*N*-(thiophen-2-ylmethyl)acetamido)propanoic acid (8): To a solution of compound **7** (1.269 g) in THF (10 mL) a solution of LiOH in water (1 M, 20 mL, 20 mmol) was added and the resulting mixture was kept under stirring for 1 h. When the reaction was completed, the solvent was evaporated and an HCl solution (2 M) was added until the formation of a white precipitate. The resulting suspension was then partitioned between EtOAc and water. The aqueous phase was extracted with (x2), the organic phase dried over Na_2SO_4 and concentrated under reduced pressure. The final product was obtained as a white solid in a quantitative yield. ^{1}H NMR (400 MHz, DMSO) δ 12.06–11.97 (br s, 1H), 8.25–8.06 (m, 2H), 8.00–7.90 (m, 1H), 7.42–7.31 (m, 1H), 7.30–7.08 (m, 3H), 6.96–6.78 (m, 3H), 6.76–6.67 (m, 1H), 6.62–6.54 (m, 1H), 5.75–5.58 (m, 1H) 4.62–4.45 (m, 2H), 3.53–3.44 (m, 3H), 3.26–3.13 (m, 2H), 2.38–1.74 (m, 2H). ^{13}C NMR (100 MHz, DMSO) δ 172.37, 168.57, 161.86, 155.12, 141.68, 139.78, 139.17, 132.11, 130.88, 130.60, 129.90, 128.61, 126.93, 126.44, 126.19, 123.54, 123.38, 123.20, 120.62, 116.96, 110.70, 55.43, 50.32, 44.22, 41.72, 31.85.

Acknowledgements

This work was funded by the European Union's Horizon 2020 research and innovation programme under the Marie Skłodowska Curie grant agreement No 765581 (PhD4Glyco-Drug Innovative Training Network). We thank OpenEye Scientific Software, Santa Fe, NM., for free academic licenses for the use of their software.

Conflict of Interest

The authors declare no conflict of interest.

Data Availability Statement

The data that support the findings of this study are available in the supplementary material of this article.

Keywords: O-GlcNAcylation · scaffold hopping · molecular docking · virtual screening · enzyme inhibition

[1] M. R. Bond, J. A. Hanover, *Annu. Rev. Nutr.* **2013**, *33*, 205–229.
[2] S. Özcan, S. S. Andrali, J. E. L. Cantrell, *Biochim. Biophys. Acta Gene Regul. Mech.* **2010**, *1799*, 353–364.
[3] G. W. Hart, *J. Biol. Chem.* **2019**, *294*, 2211–2231.
[4] M. Aquino-Gil, A. Pierce, Y. Perez-Cervera, E. Zenteno, T. Lefebvre, *Biochem. Soc. Trans.* **2017**, *45*, 365–370.
[5] H. G. Selnick, J. F. Hess, C. Tang, K. Liu, J. B. Schachter, J. E. Ballard, J. Marcus, D. J. Klein, X. Wang, M. Pearson, et al., *J. Med. Chem.* **2019**, *62*, 10062–10097.
[6] V. S. Borodkin, K. Rafie, N. Selvan, T. Aristotelous, I. Navratilova, A. T. Ferenbach, D. M. F. van Aalten, *ACS Chem. Biol.* **2018**, *13*, 1353–1360.
[7] L. VandeVrede, A. L. Boxer, M. Polydoro, *Neurosci. Lett.* **2020**, *731*, 134919.
[8] L. K. Abramowitz, J. A. Hanover, *FEBS Lett.* **2018**, *592*, 3943–3949.
[9] C. M. Joiner, Z. G. Levine, C. Aonbangkhen, C. M. Woo, S. Walker, *J. Am. Chem. Soc.* **2019**, *141*, 12974–12978.
[10] V. Makwana, P. Ryan, B. Patel, S. A. Dukie, S. Rudrawar, *Biochim. Biophys. Acta Gen. Subj.* **2019**, *1863*, 1302–1317.
[11] V. M. Pravata, V. Muha, M. Gundogdu, A. T. Ferenbach, P. S. Kakade, V. Vandadi, A. C. Wilmes, V. S. Borodkin, S. Joss, M. P. Stavridis, et al., *Proc. Nat. Acad. Sci.* **2019**, *116*, 14961–14970.
[12] A. C. Leney, D. El Atmioui, W. Wu, H. Ovaa, A. J. R. Heck, *Proc. Nat. Acad. Sci.* **2017**, *114*, E7255–E7261.
[13] S. A. M. van der Laarse, A. C. Leney, A. J. R. Heck, *FEBS J.* **2018**, *285*, 3152–3167.
[14] J. Shi, T. Tomašič, S. Sharif, A. J. Brouwer, M. Anderluh, R. Ruijtenbeek, R. J. Pieters, *FEBS Lett.* **2017**, *591*, 1872–1883.
[15] J. Shi, S. Sharif, R. Ruijtenbeek, R. J. Pieters, *PLoS One* **2016**, *11*, e0151085.
[16] S. Sharif, J. Shi, M. Bourakba, R. Ruijtenbeek, R. J. Pieters, *Anal. Biochem.* **2017**, *532*, 12–18.
[17] J. Shi, R. Ruijtenbeek, R. J. Pieters, *Glycobiology* **2018**, *28*, 814–824.
[18] Z. Wang, N. D. Udeshi, C. Slawson, P. D. Compton, K. Sakabe, W. D. Cheung, J. Shabanowitz, D. F. Hunt, G. W. Hart, *Sci. Signaling* **2010**, *3*, DOI 10.1126/scisignal.2000526.
[19] S. Wang, X. Huang, D. Sun, X. Xin, Q. Pan, S. Peng, Z. Liang, C. Luo, Y. Yang, H. Jiang, et al., *PLoS One* **2012**, *7*, DOI 10.1371/journal.-pone.0037427.
[20] P. A. Schwein, C. M. Woo, *ACS Chem. Biol.* **2020**, *15*, 602–617.
[21] H. Zhang, T. Tomašič, J. Shi, M. Weiss, R. Ruijtenbeek, M. Anderluh, R. J. Pieters, *MedChemComm* **2018**, *9*, 883–887.
[22] V. S. Borodkin, M. Schimpl, M. Gundogdu, K. Rafie, H. C. Dorfmueller, D. A. Robinson, D. M. F. van Aalten, *Biochem. J.* **2014**, *457*, 497–502.
[23] T. M. Gloster, W. F. Zandberg, J. E. Heinonen, D. L. Shen, L. Deng, D. J. Vocadlo, *Nat. Chem. Biol.* **2011**, *7*, 174–181.
[24] R. F. Ortiz-Meoz, J. Jiang, M. B. Lazarus, M. Orman, J. Janetzko, C. Fan, D. Y. Duveau, Z.-W. Tan, C. J. Thomas, S. Walker, *ACS Chem. Biol.* **2015**, *10*, 1392–1397.
[25] S. E. S. Martin, Z.-W. Tan, H. M. Itkonen, D. Y. Duveau, J. A. Paulo, J. Janetzko, P. L. Boutz, L. Törk, F. A. Moss, C. J. Thomas, et al., *J. Am. Chem. Soc.* **2018**, *140*, 13542–13545.
[26] Y. Liu, Y. Ren, Y. Cao, H. Huang, Q. Wu, W. Li, S. Wu, J. Zhang, *Sci. Rep.* **2017**, *7*, 1–11.
[27] R. Trapannone, K. Rafie, D. M. F. van Aalten, *Biochem. Soc. Trans.* **2016**, *44*, 88–93.
[28] E. M. Loi, M. Weiss, S. Pajk, M. Gobec, T. Tomasic, R. J. Pieters, M. Anderluh, *Molecules* **2020**, *25*, 3381.
[29] S. O. Albuquerque, T. G. Barros, L. R. S. Dias, C. H. d. S. Lima, P. H. R. d. A. Azevedo, L. A. P. Flores-Junior, E. G. dos Santos, H. F. Loponte, S. Pinheiro, W. B. Dias, et al., *Eur. J. Pharm. Sci.* **2020**, *154*, 105510.
[30] M. R. Berthold, N. Cebron, F. Dill, G. Di Fatta, T. R. Gabriel, F. Georg, T. Meinl, P. Ohl, C. Sieb, B. Wiswedel, *4th Int. Ind. Simul. Conf. 2006, ISC 2006* **2006**, 58–61.
[31] "OMEGA 4.2.0.1: OpenEye Scientific Software, Santa Fe, NM. http://www.eyesopen.com.," **n.d.**
[32] P. C. D. Hawkins, A. G. Skillman, G. L. Warren, B. A. Ellingson, M. T. Stahl, *J. Chem. Inf. Model.* **2010**, *50*, 572–584.
[33] E. M. Loi, T. Tomašic, C. Balsollier, K. van Eekelen, M. Weiss, M. G. Alteen, D. J. Vocadlo, R. J. Pieters, M. Anderluh, *Molecules* **2022**, *27*, 1996.
[34] M. McGann, *J. Comput.-Aided Mol. Des.* **2012**, *26*, 897–906.
[35] M. G. Alteen, C. Gros, R. W. Meek, D. A. Cardoso, J. A. Busmann, G. Sangouard, M. C. Deen, H. Y. Tan, D. L. Shen, C. C. Russell, et al., *Angew. Chem. Int. Ed. Engl.* **2020**, *59*, 9601–9609.

Manuscript received: January 2, 2023
Revised manuscript received: January 27, 2023
Accepted manuscript online: February 8, 2023
Version of record online: March 2, 2023